

1 **Amplified seasonality in western Europe in a warmer world**

2 Niels J. de Winter<sup>1,2</sup>, Julia Tindall<sup>3</sup>, Andrew L.A. Johnson<sup>4</sup>, Barbara Goudsmit-Harzevoort<sup>5,6</sup>, Nina Wichern<sup>7</sup>,  
3 Pim Kaskes<sup>2,8</sup>, Philippe Claeys<sup>2</sup>, Fynn Huygen<sup>9</sup>, Sonja van Leeuwen<sup>5</sup>, Brett Metcalfe<sup>1,10</sup>, Pepijn Bakker<sup>1</sup>, Stijn  
4 Goolaerts<sup>11</sup>, Frank Wesselingh<sup>12</sup>, Martin Ziegler<sup>6</sup>

5 <sup>1</sup>Department of Earth Sciences, Vrije Universiteit Amsterdam, the Netherlands

6 <sup>2</sup>Archaeology, Environmental Changes and Geochemistry group, Vrije Universiteit Brussel, Belgium

7 <sup>3</sup>School of Earth and Environment, University of Leeds, United Kingdom

8 <sup>4</sup>College of Science and Engineering, University of Derby, United Kingdom

9 <sup>5</sup>Department of Estuarine and Delta Systems, Royal Netherlands Institute for Sea Research, the  
10 Netherlands

11 <sup>6</sup>Department of Earth Sciences, Utrecht University, the Netherlands

12 <sup>7</sup>Institut für Geologie und Paläontologie, Universität Münster, Germany

13 <sup>8</sup>Laboratoire G-Time, Université Libre de Bruxelles, Belgium

14 <sup>9</sup>Institut für Geowissenschaften, Universität Kiel, Germany

15 <sup>10</sup>Laboratory of Systems and Synthetic Biology, Wageningen University & Research, the Netherlands

16 <sup>11</sup>Directorate Earth and History of Life, Royal Belgian Institute for Natural Sciences, Brussels, Belgium

17 <sup>12</sup>Naturalis Biodiversity Center, Leiden, Netherlands

18

19 This is a non-peer reviewed pre-print. This manuscript has been submitted for publication in the journal  
20 Science Advances.

21 **Abstract**

22 Documenting the seasonal temperature cycle constitutes an essential step towards mitigating risks  
23 associated with extreme weather events in a future warmer world. The mid-Piacenzian Warm Period  
24 (mPWP), 3.3 – 3.0 million years ago, featured global temperatures approximately 3°C above pre-industrial  
25 levels. It represents an ideal period for directed paleoclimate reconstructions equivalent to model  
26 projections for 2100 under moderate Shared Socioeconomic Pathway SSP2-4.5. Here, seasonal clumped  
27 isotope analyses in fossil mollusc shells from the North Sea are presented to test Pliocene Model  
28 Intercomparison Project 2 outcomes. Joint data and model evidence reveals enhanced summer warming  
29 ( $+4.2 \pm 2.6$  °C) compared to winter ( $+2.2 \pm 2.0$ °C) during the mPWP, equivalent to SSP2-4.5 outcomes for  
30 future climate. We show that Arctic Amplification of global warming weakens mid-latitude summer  
31 circulation while intensifying seasonal contrast in temperature and precipitation, leading to an increased  
32 risk of summer heatwaves and other extreme weather events in Europe's future.

33

34 **Teaser:** Seasonal scale climate reconstructions and models show that CO<sub>2</sub> increase warms up Europe's  
35 summers faster than its winters.

## 36 Introduction

37 The mid-Piacenzian Warm Period (mPWP) represents an interval with global temperatures estimated on  
38 average 3.2°C (1.7 – 5.2°C) higher than pre-industrial climate due predominantly to elevated atmospheric  
39 CO<sub>2</sub> concentrations (~400 ppmV)<sup>1-3</sup>. Temperatures during this period closely resemble the mean global  
40 temperatures projected for the year 2100 following the Shared Socioeconomic Pathway (SSP) 2-4.5<sup>4-7</sup>, the  
41 SSP scenario most likely to occur given the current global climate policy<sup>8</sup>. The Pliocene Model  
42 Intercomparison Project 2 (PlioMIP2) consortium has targeted the mPWP using an ensemble of General  
43 Circulation Models<sup>9</sup>. This allows a detailed data-model comparison, which is essential for assessing the  
44 performance of climate models simulating climate scenarios with higher temperatures than represented  
45 in instrumental records, similar to conditions which will most likely define future climate on Earth<sup>2,5</sup>.

46 One region under extreme threat in a global warming scenario is the Arctic region that is anticipated to  
47 warm up two to four times faster than the global average, a phenomenon called Arctic Amplification<sup>10</sup>.  
48 Model experiments using future CO<sub>2</sub> forcing scenarios imply that Arctic Amplification caused by global  
49 warming of mPWP magnitude might impact the storm-track affected regions of European climate by  
50 weakening atmospheric summer circulation<sup>11</sup>, significantly reducing summer cloud cover<sup>12</sup> and leading to  
51 persistently elevated summer temperatures and droughts over Europe<sup>13,14</sup>. Considering these “dynamic”  
52 drivers of summer weather extremes, related to changes in atmospheric circulation, in future projections  
53 would result in more extreme weather variability than expected based on “thermodynamic” drivers based  
54 on temperature changes alone<sup>14</sup>. Given this season-specific response of weather patterns to warming,  
55 seasonal scale reconstructions of mPWP climate are crucial to validate climate model simulations and  
56 improve our understanding of the impact of higher atmospheric greenhouse gas concentrations on  
57 European climate.

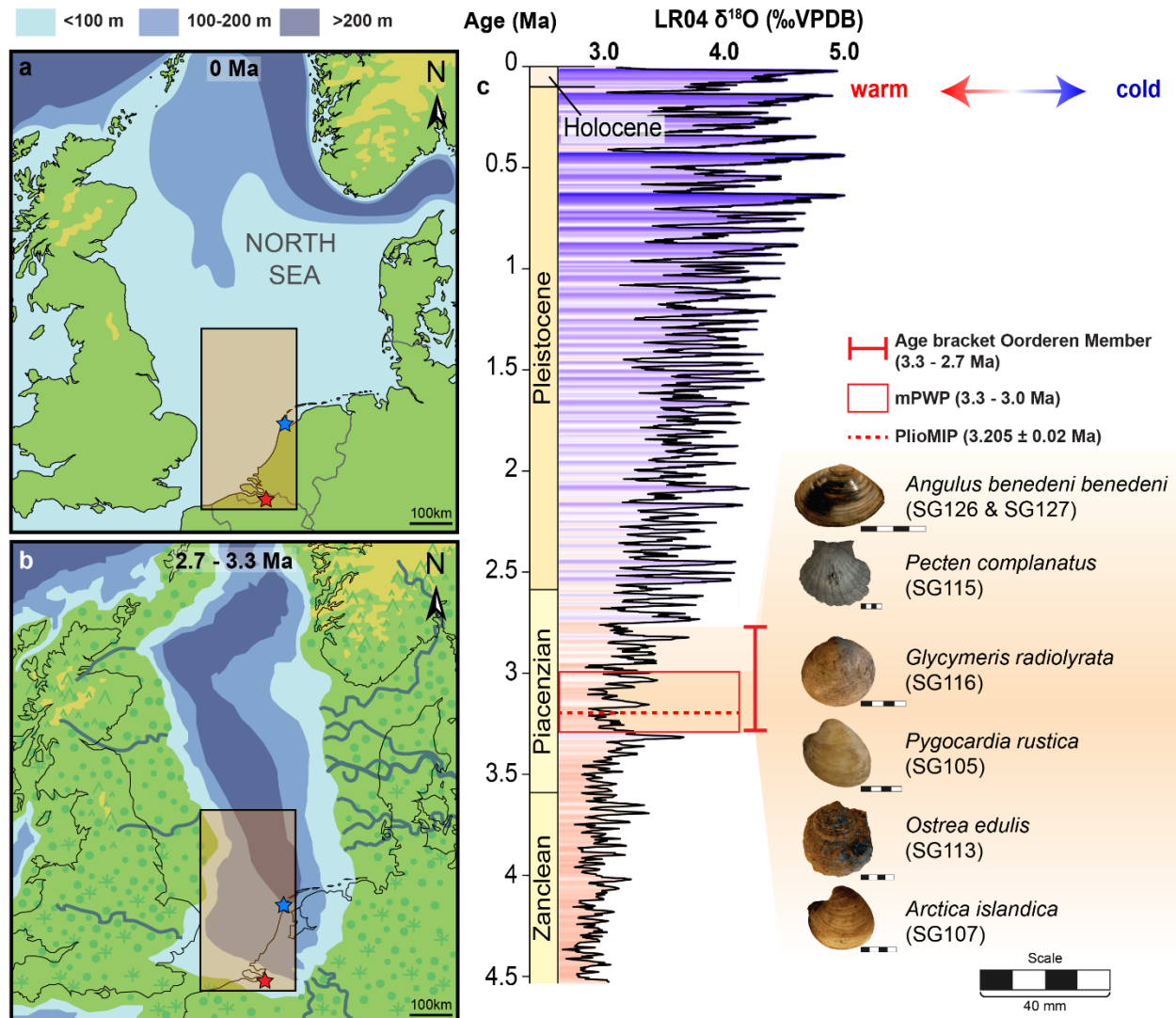
58 Yet, climate proxy records from pelagic sediment cores, which form the predominant method of  
59 estimating mPWP temperatures<sup>15-17</sup>, rarely resolve seasonal scale variability in the temperature cycle due  
60 to low temporal resolution. Furthermore, short-lived marine organisms that make up pelagic sediments  
61 preferentially grow only during specific seasons with favourable conditions. This seasonal bias places  
62 considerable uncertainty on marine climate reconstructions and data-model comparisons based on  
63 common temperature proxies, such as Mg/Ca and stable isotope ratios in foraminifera<sup>18</sup>, TEX<sub>86</sub> from  
64 membrane lipids in Crenarchaeota<sup>19</sup> and U<sub>37</sub><sup>K</sup> based on ketones in haptophyte algae<sup>20</sup>. Likewise, previous  
65 studies have highlighted the challenge of reconciling seasonal-scale mPWP climate reconstructions and  
66 models of terrestrial seasonality<sup>21</sup>.

67 One approach to facilitate seasonal data-model comparison is to use marine molluscs that record daily to  
68 decadal scale variability in the chemistry of their calcium carbonate shells<sup>22-25</sup>, and preserve this high-  
69 resolution environmental variability on geological timescales<sup>26-28</sup>. Climate reconstructions from mid-  
70 latitude shelf seas, where these molluscs are common, are instrumental in assessing the impact of  
71 warming on the seasonal scale, because these regions experience high seasonal temperature contrast and  
72 their ecosystems are strongly impacted by climate change<sup>29-32</sup>. Going a step further, by using the clumped  
73 isotope composition of shell carbonate, it becomes possible to reconstruct seasonal temperature changes  
74 of the water in which molluscs grow without relying on uncertain assumptions of the isotopic composition  
75 of past ocean water, leading to accurate reconstructions of past seasonality<sup>26,33,34</sup>.

76 We present seasonal sea surface temperature (SST) reconstructions based on clumped isotope analyses  
77 from well-preserved fossil mollusc shells originating from the Lillo Formation (northern Belgium; see

78 **Methods**). These sediments were deposited below fair-weather wave base (30 – 50 m water depth ) in  
79 the southern North Sea (SNS) during the warm, high-sea level intervals during and slightly after the mPWP  
80 (2.7 – 3.3 Ma<sup>35,36</sup>; **Fig. 1**). These shells record marine temperatures in the mPWP southern North Sea<sup>37</sup>, an  
81 important model ecosystem for temperate shelf seas worldwide<sup>38</sup>. Based on the observation of  
82 sedimentary structures indicative of strong tidal mixing<sup>39</sup>, the absence of dysoxic fauna (see **Online**  
83 **Methods**) and the observation of high spring temperatures (see **Results; Fig. 2-3**), it seems likely that the  
84 shells used in this study record conservative summer temperatures close to the true summer SST during  
85 the mPWP.

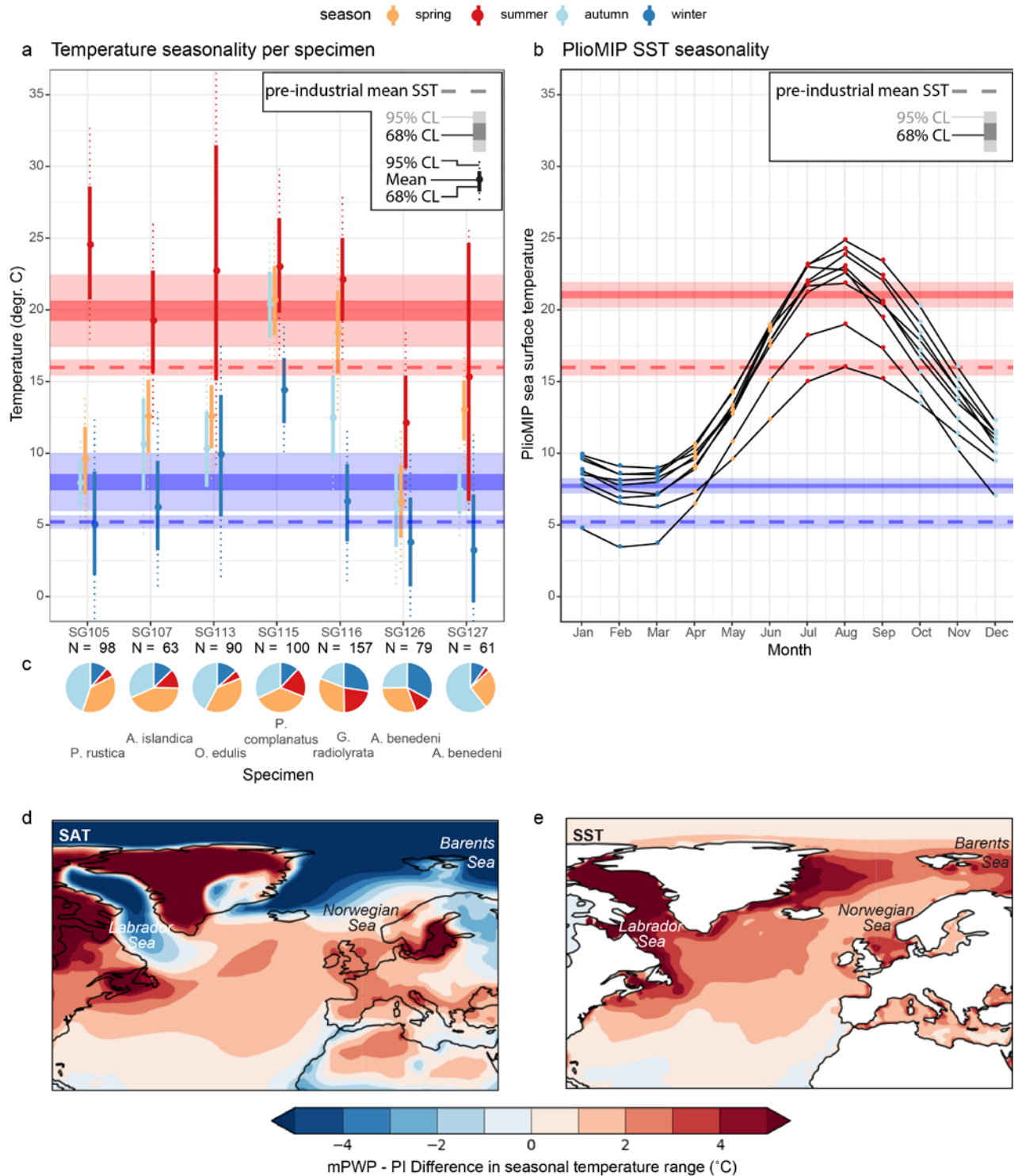
86 We directly compare our seasonal SST reconstructions with the results of PLIOMIP2 ensemble model  
87 simulations of seasonal temperature changes in the SNS during the mPWP as well as with instrumental  
88 temperature records in the region and Coupled Model Intercomparison Project Phase 6 (CMIP6) SSP2-4.5  
89 projections of European climate for the year 2100. This approach offers a detailed glimpse of the potential  
90 future climate in Europe under a moderate emission scenario.



91

92 **Figure 1: Locality of the study site and long-term climate context.** Maps of northwestern Europe showing  
 93 the present (a) and estimated mPWP (b; after<sup>35,37,40</sup>) SNS bathymetry. The locality of fossil shells (red star),  
 94 the local temperature record (blue star) and the area containing the SNS data integrated from extended  
 95 reconstructed SST (ERSSTv5), PlioMIP2 and CMIP6 models (black rectangle with orange filling; 51-55°N, 2-  
 96 4°E; Fig. 2-3) is indicated. (c) Age bracket of the Oorderen Member (Lillo formation) containing the mollusc  
 97 specimens<sup>35</sup> (orange shaded region) relative to the mPWP<sup>41</sup> (red box) and PlioMIP2<sup>1</sup> interval (dashed red  
 98 line) and the global benthic foraminifera oxygen isotope stack<sup>42</sup> with relative temperature change  
 99 indicated. Note that mollusc specimens likely originate from highstand (i.e., warmer) periods within the  
 100 age bracket (see **Online Methods**).

101



102

103 **Figure 2: Data-model comparison.** (a) Weighted mean seasonal temperatures per specimen (filled circles  
 104 with solid and dotted vertical lines indicating 68% and 95% confidence levels, respectively) and summer  
 105 and winter temperatures based on the complete dataset (horizontal shaded bars in red and blue,  
 106 respectively) with propagated uncertainties (68% and 95% confidence level; see **Online Methods**). Dashed  
 107 horizontal lines in the same colours indicate mean pre-industrial SNS SST. (b) Local monthly SST outcomes

108 of individual PLIOMIP2 models with winter (Jan-Mar; blue) and summer (Jul-Sep; red) temperature  
109 estimates (horizontal shaded bars showing 68% and 95% CL). Dashed lines in the same colours indicate  
110 mean SST outcomes (with uncertainty; 95% CL<sup>9</sup>) from pre-industrial control simulations using the same  
111 models. (c) Clumped isotope sample sizes and seasonal representation of samples per specimen. Panel  
112 **(d)** and **(e)** show spatial variability in the difference in seasonal contrast (July - January) in surface air  
113 temperature (SAT; **d**) and SST (**e**), respectively, between PLIOMIP2 multi-model mean mPWP runs and  
114 PLIOMIP2 PI control runs of the same models.

## 115 Results

### 116 *Data-model agreement on enhanced summer warming in the North Sea*

117 Aggregated results from all bivalve specimens give weighted winter ( $8.0 \pm 2.0^\circ\text{C}$ ), spring ( $13.1 \pm 1.6^\circ\text{C}$ ),  
118 summer ( $19.9 \pm 2.5^\circ\text{C}$ ) and autumn ( $10.0 \pm 1.4^\circ\text{C}$ ) SST averages during the mPWP in the SNS (**Fig. 2a**). The  
119 reconstructed winter and summer temperatures agree with winter (January-March;  $7.7 \pm 0.5^\circ\text{C}$ ) and  
120 summer temperatures (July-September;  $21.1 \pm 0.9^\circ\text{C}$ ) from aggregated PLIOMIP2 model results (**Fig. 2b**).  
121 Both reconstructed and modelled winter and summer temperatures are significantly higher than winter  
122 ( $5.2 \pm 0.9^\circ\text{C}$ ) and summer temperatures ( $16.0 \pm 0.6^\circ\text{C}$ ) in pre-industrial (280 ppmV CO<sub>2</sub>) PLIOMIP2 control  
123 runs and instrumental records (**Fig. 2a-b**). Our reconstructions yield  $2.2 \pm 2.0^\circ\text{C}$  warmer winters and  $4.2 \pm$   
124  $2.6^\circ\text{C}$  warmer summers during the mPWP compared to mean winter ( $5.8 \pm 0.3^\circ\text{C}$ ) and summer  
125 temperatures ( $15.7 \pm 0.4^\circ\text{C}$ ) in the SNS over the period 1854-1900 CE (**Fig. 3a**; based on NOAA ERSSTv5<sup>43</sup>).

### 126 *Locally elevated spring temperatures*

127 Intriguingly, mollusc-based reconstructions yield significantly higher spring (April-June;  $13.1 \pm 1.6^\circ\text{C}$ ) than  
128 autumn (October-December;  $10.0 \pm 1.4^\circ\text{C}$ ) temperatures during the mPWP. This contrasts with regional  
129 SNS SST averages from both pre-industrial (spring:  $9.4 \pm 1.0^\circ\text{C}$ ; autumn:  $10.3 \pm 0.8^\circ\text{C}$ ) and mPWP (spring:  
130  $13.0 \pm 1.2^\circ\text{C}$ ; autumn:  $13.6 \pm 1.1^\circ\text{C}$ ) PLIOMIP2 model runs as well as ERSST SNS SST averages (spring:  $9.5 \pm$   
131  $0.3^\circ\text{C}$ ; autumn:  $10.9 \pm 0.3^\circ\text{C}$ ), which consistently yield higher temperatures in autumn compared to spring.  
132 Contrarily, local pre-industrial instrumental SST time series from the SNS coast (NIOZ monitoring station  
133 on the island of Texel, NW Netherlands<sup>44</sup>; see **Fig. 1a-b**; **Online Methods**) do exhibit significantly elevated  
134 spring temperatures ( $11.4 \pm 0.5^\circ\text{C}$ ) compared to autumn ( $9.1 \pm 0.5^\circ\text{C}$ ). Shallow coastal waters, such as the  
135 tidal flats of the Wadden Sea close to the NIOZ monitoring station, are highly responsive to air  
136 temperature, which leads to elevated sea surface temperatures in the spring season, while more offshore  
137 areas of the North Sea have higher thermal inertia, explaining elevated autumn temperatures<sup>44</sup>. The  
138 elevated spring and reduced autumn SST reconstructions thus highlight that the mollusc shells record  
139 detailed seasonal SST variability in the coastal SNS during the mPWP.

### 140 *Inter-specimen variability*

141 Reconstructed seasonal temperatures vary between fossil shell specimens, with some species recording  
142 warmer temperatures (e.g. *Pecten complanatus*; SG115; winter:  $14.4 \pm 4.3^\circ\text{C}$ , summer:  $23.0 \pm 4.2^\circ\text{C}$ ) and  
143 others cooler temperatures (e.g. *Angulus benedeni benedeni*; SG126 & SG127; winter:  $3.2 \pm 6.7^\circ\text{C}$ ,  
144 summer:  $13.0 \pm 2.1^\circ\text{C}$ ; **Fig. 2a**). These inter-species differences probably occur due to the occurrence of  
145 growth stops, and variations in growth rates between seasons (**Fig. 2c**) and between consecutive growth  
146 years (see **Supplementary Information Figure S13-S26**), which dampen seasonality due to the averaging  
147 of samples around the seasonal extreme. In addition, variability between specimens may arise from  
148 differences in the seasonal temperature range within their age range (2.7 – 3.3 Ma; see **Fig. 1c**). Our  
149 weighed averages of summer and winter temperatures (**Fig. 2a**) ensures this inter-specimen variability  
150 does not bias the reconstructions.

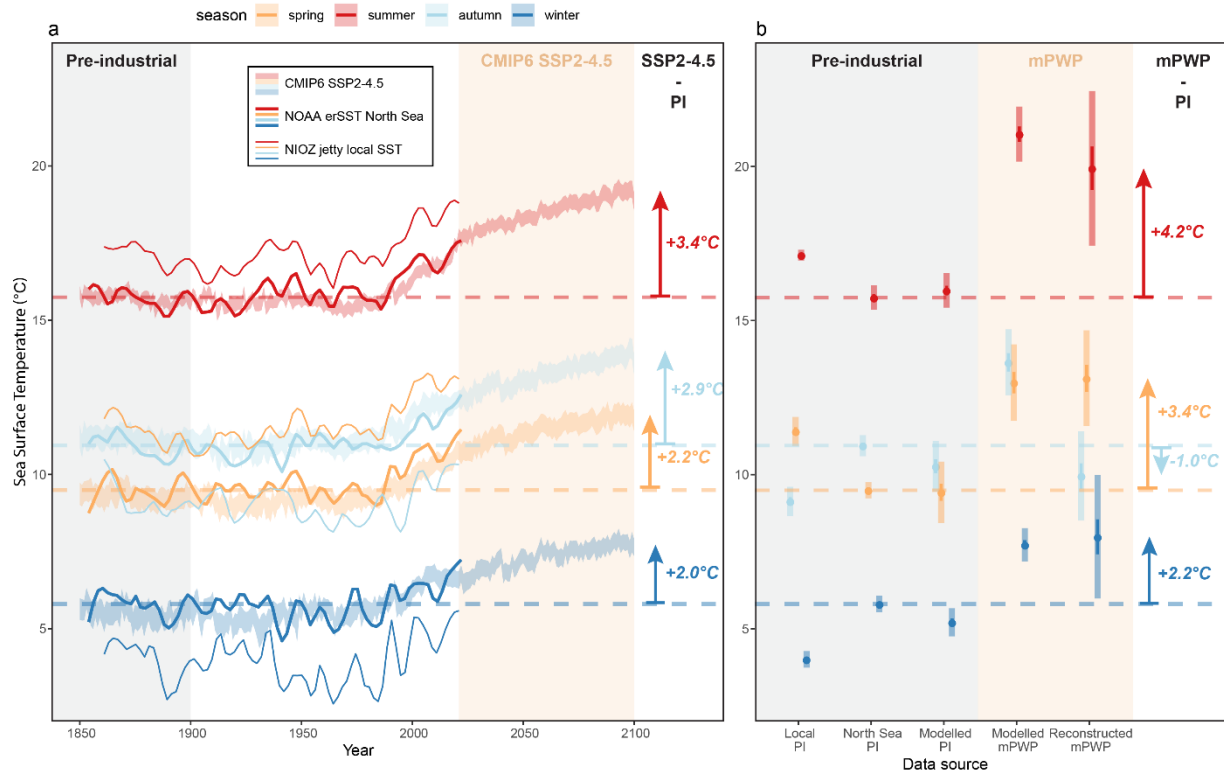
### 151 *PLIOMIP2 models reproduce SST seasonality in the modern North Sea*

152 Transient simulations of SNS SST seasonality from before the Industrial Revolution (1850 CE) to present-  
153 day (2023 CE) by the CMIP6 model ensemble<sup>6</sup> mimic historical SST records from the region<sup>43</sup> (**Fig 3a**).  
154 Seasonal SNS SST simulations by the PlioMIP2 model ensemble under preindustrial radiative forcing<sup>9</sup>

155 (winter:  $5.2 \pm 0.5^\circ\text{C}$ ; summer:  $16.0 \pm 0.6^\circ\text{C}$ ) closely resemble pre-industrial (1850 – 1900 CE) CMIP6  
156 seasonal SNS SST simulations (winter:  $5.5 \pm 0.3^\circ\text{C}$ ; summer:  $15.7 \pm 0.7^\circ\text{C}$ ) and historical winter ( $5.8 \pm 0.3^\circ\text{C}$ )  
157 and summer SNS SST ( $15.7 \pm 0.4^\circ\text{C}$ ) records<sup>43</sup> (**Fig. 3b**). Local SST records from the NIOZ monitoring station  
158 on Texel<sup>44</sup> reveal slightly higher seasonal SST ranges (winter:  $4.0 \pm 0.3^\circ\text{C}$ ; summer:  $17.1 \pm 0.2^\circ\text{C}$ ; **Fig. 3b**)  
159 which are well explained by their coastal location (see above). This agreement shows that PLIOMIP2  
160 models successfully reproduce summer and winter SSTs in the SNS.

#### 161 *The mid- to high latitude seasonal temperature response to mPWP-like warming*

162 Maps of PLIOMIP2 seasonal SST outcomes show that the enhanced seasonal contrast observed in our  
163 reconstructions is present throughout the mid to high latitudes in the North Atlantic (**Fig. 2e**). Enhanced  
164 SST seasonality is more pronounced in areas which are characterized by high seasonal contrast in surface  
165 air temperature and cold winters (e.g. Labrador Sea and Barents Sea) than in regions with milder winters  
166 (e.g. Norwegian Sea). Contrarily, surface air temperature (SAT) only shows enhanced seasonal contrast in  
167 the mid-latitudes under mPWP conditions (**Fig. 2d**). Areas with the strongest enhanced seasonal SST  
168 contrast (e.g. Labrador Sea and Barents Sea; **Fig. 2e**) show a reduced seasonal SAT contrast under mPWP  
169 conditions compared to the PI control runs (**Fig. 2d**). PLIOMIP2 model simulations of sea ice extent  
170 (**Supplementary Information Figure S33**) show that these regions where the SST and SAT seasonality  
171 respond differently to mPWP-scale warming are characterized by winter sea ice cover in PI runs. They lose  
172 much of their winter sea ice under mPWP conditions. A 53% decrease in mean annual sea ice extent during  
173 the mPWP compared to pre-industrial climate is simulated in PLIOMIP2 models<sup>45</sup>. Contrarily, areas with  
174 enhanced summer warming in both SST and SAT are sea-ice free year-round in both mPWP and PI model  
175 runs. SAT seasonality over land (both in North America and Europe; **Fig. 2d**) is enhanced in both mid and  
176 high latitudes, following the SST pattern. At the same time, PLIOMIP2 model outcomes show that summer  
177 cloud cover is severely reduced in the mid-latitudes of the North Atlantic, where both SST and SAT  
178 seasonality is enhanced (**Supplementary Information Figure S34-S35**).



179

180 **Figure 3: Pliocene reconstructions inform future climate projections (a)** Seasonal local (NIOZ jetty, Texel,  
 181 NL) SST measurements (thin solid lines; LOESS smoothed with span of 10% of the record), NOAA ERSSSTv5  
 182 SNS SST averages (thick solid lines; LOESS smoothed with span of 10% of the record) and CMIP6 SSP2-4.5  
 183 scenario transient SNS SST simulations (shaded area) between 1850 and 2100. Arrows and figures on the  
 184 right indicate temperature differences between CMIP6 SSP2-4.5 projections for 2100 CE and pre-industrial  
 185 SNS SSTs (dashed lines) **(b)** Pre-industrial (PI; before 1900 CE) seasonal SST averages based on historical  
 186 SST records (NOAA ERSSSTv5<sup>43</sup> SNS averages and NIOZ jetty local record<sup>44</sup>) and PlioMIP2 pre-industrial  
 187 model outcomes are compared with mPWP seasonality based on PlioMIP2 mPWP model simulations and  
 188 mollusc-based reconstructions. Arrows and figures on the right indicate seasonal temperature differences  
 189 between mollusc-based mPWP temperature reconstructions and pre-industrial SNS SST (dashed lines).

190

## 191 Discussion

192 Recent terrestrial mPWP data-model comparisons highlight that PLIOMIP2 models cannot reproduce the  
193 full extent of the mPWP warming that data suggest<sup>2,21,46</sup>. Likewise, in both the pelagic and terrestrial realm,  
194 reconstruction of the full seasonal cycle is challenging due to proxy limitations<sup>2,21</sup>. Detailed temperature  
195 monitoring studies show that shallow marine temperatures are strongly linked to air temperatures and  
196 local weather systems<sup>47</sup>. Together with the enhanced occurrence of summer stratification in warmer  
197 climates<sup>24,48,49</sup>, a change in atmospheric circulation patterns may drive the summer increase in SST during  
198 the mPWP and in future climate observed in data and models (**Fig. 2-3**). Since the seasonal cycle is much  
199 more pronounced in the terrestrial realm, this limitation could explain part of the large seasonal data-  
200 model mismatch in terrestrial Northern Hemisphere high latitudes<sup>21</sup>.

201 PLIOMIP2 models closely agree with mollusc-based reconstructions of SNS summer and winter SST during  
202 the mPWP (**Fig. 2 & 3b**). The summer warming observed in SST data and model outcomes is also reflected  
203 in PLIOMIP2 SAT seasonality in the SNS region (**Fig. 2d; Supplementary information Figure S37**). This  
204 highlights that PLIOMIP2 models can reconstruct seasonal SST variability in the North Atlantic, despite the  
205 difficulties with terrestrial data-model comparisons<sup>21</sup>. However, large inter-model variability in regions  
206 with poor data-model agreement suggests that structural model uncertainties also contribute to the  
207 mismatch<sup>21</sup>.

208 The agreement between PLIOMIP2 pre-industrial control simulations and present-day climate  
209 (represented in CMIP6 models and instrumental records; **Fig. 3**)<sup>1,9,50</sup> lends confidence to the application  
210 of mPWP reconstructions and model simulations to better understand the seasonal impact of moderate  
211 global warming on future European climate. The seasonal-scale data-model agreement in the SNS,  
212 situated between the pelagic and terrestrial realms, both for present-day and mPWP climate, sheds new  
213 light on the seasonal response to warmer climate in the mid latitudes: The unique potential of marine  
214 molluscs to record seasonal-scale SST variability in coastal regions<sup>28,51</sup> in combination with the strong  
215 relationship between mid-latitude coastal SST and SAT<sup>47,52</sup> (see **Fig. 2d** and **Supplementary Information**  
216 **Figure S28-S32**) highlights the key role of seasonally resolved shallow marine climate archives for better  
217 understanding past and future climates.

218 Our mollusc-based data and PLIOMIP2 model estimates of mPWP SST seasonality resemble projections of  
219 future (2081 – 2100 CE) SNS winter ( $7.7 \pm 0.3^\circ\text{C}$ ) and summer SST ( $19.1 \pm 0.5^\circ\text{C}$ ; **Fig. 3a**) by transient CMIP6  
220 model simulations of the “middle-of-the-road” SSP2-4.5 scenario<sup>50</sup> (**Fig. 3**). Note that these are two  
221 different climate scenarios: CMIP6 represents a transient climate disturbance, while the mPWP  
222 simulations and reconstructions sample an equilibrated climate under long-term atmospheric CO<sub>2</sub> forcing  
223 of 400 ppmV<sup>9</sup>. The difference is evident from atmospheric pCO<sub>2</sub> projections of ~600 ppmV in 2100 CE and  
224 ~580 ppmV on the long term (2500 CE) under SSP2-4.5, which significantly exceed the mPWP estimate of  
225 ~400 ppmV<sup>3,5</sup>. Notwithstanding this difference, the results of our data-model comparison and the  
226 similarity of the SSP2-4.5 scenario to the current global emission trajectory<sup>4</sup> show that the mPWP presents  
227 valuable lessons for climate in Europe by the end of this century and that models are able to project  
228 seasonal climate in this region in a warmer world.

229 The spatial variability in seasonal response to mPWP warming of SST and SAT reveals a clear signature of  
230 sea ice extent: SST and SAT respond in opposite directions to mPWP warming in the higher latitude areas  
231 that lose winter sea ice cover under mPWP conditions (**Fig. 2d-e**; e.g. Labrador Sea and Barents Sea;  
232 **Supplementary Information Figure S33**). The loss of winter sea ice in a mPWP-like climate scenario

233 facilitates heat transfer from the upper ocean to the lower atmosphere in winter, cooling the upper ocean  
234 in winter (enhancing SST seasonality) and warming the lower atmosphere (reducing SAT seasonality)<sup>45</sup>.  
235 This effect explains why higher latitudes are more impacted by the sea ice-albedo feedback which changes  
236 due to a reduction in sea ice extent under the mPWP-like conditions<sup>53,54</sup> and in future climate scenarios<sup>55</sup>.  
237 In these regions, Arctic Amplification is expected to cause winter SAT to warm faster than other  
238 regions<sup>10,56</sup>, while SST actually shows a summer warming effect in both the high and the mid latitudes.

239 This hypothesis is supported by climate models showing that Arctic Amplification reduces the latitudinal  
240 SAT gradient in warmer climates<sup>10</sup>. This weakens the mid-latitude atmospheric summer circulation,  
241 causing a weakening of storm tracks, with lower cyclone activity over Europe, more persistent weather  
242 and a reduction in summer cloud cover<sup>11</sup>. This reduction in cloud cover over temperate latitudes of the  
243 North Atlantic is also simulated in PlioMIP2 model outcomes (**Supplementary Information Figure S35**)<sup>13</sup>.  
244 Recent observations from various parts of the North Atlantic region suggest that circulation changes are  
245 already enhancing summer warming and prolonging heat waves through low cyclone activity, low cloud  
246 cover and more persistent weather<sup>12,57,58</sup>. In the winter months, zonal (westerly) wind increases,  
247 enhancing cloud cover and precipitation and suppressing winter warming<sup>13</sup>. Taken together, this change  
248 in the atmospheric circulation regime results in an increase in extreme weather conditions in Europe in  
249 both seasons, with more severe precipitation events in winter and more prolonged droughts in summer<sup>13</sup>.

250 Our data-model analysis reveals that a mPWP-scale SST increase in the SNS region causes more  
251 pronounced warming in summer (reconstructions:  $+4.2 \pm 2.6$  °C; PliOMIP2 models:  $+5.1 \pm 0.9$  °C) than in  
252 winter (reconstructions:  $+2.2 \pm 2.0$  °C; PliOMIP2 models:  $+2.5 \pm 0.5$  °C; **Fig. 3b**). Historical climate data (**Fig.**  
253 **3a**) and recent climate attribution studies<sup>59-61</sup> reveal that this trend is already underway in Europe<sup>62</sup>.  
254 Therefore, reconstructions and model simulations of mPWP seasonality reveal the impact of our current  
255 climate trajectory: Due to the hypothesized mid-latitude circulation changes, global warming is likely to  
256 regionally shift the distribution of extreme weather events on top of the overall increase in frequency and  
257 severity of these events due to the thermodynamic effect of greenhouse warming<sup>14</sup>. The seasonally  
258 asymmetric change in mid-latitude zonal circulation, even under a relatively mild mPWP-like warming  
259 scenario, renders Europe particularly vulnerable to prolonged heat and drought in summer and intense  
260 precipitation events in winter<sup>13</sup>. Enhanced summer warming in coastal regions poses a serious risk for  
261 shallow marine communities, since it leads to more frequent and extreme weather events, such as marine  
262 heatwaves<sup>29,30,59,61,63</sup>. These marine heatwaves<sup>64</sup> have recently caused mass mortality events<sup>65</sup>, mass coral  
263 bleaching<sup>66</sup> and toxic algae blooms<sup>67</sup>, severely affecting marine biodiversity. They are among the major  
264 reasons for concern related to anthropogenic climate change<sup>68</sup>. Considering the high societal and  
265 ecological importance of mid-latitude coastal regions, local data-model comparison studies of short-term  
266 variability during past climates relevant for future warming scenarios play a fundamental role in honing  
267 model projections which inform climate adaptation strategies.

268

## 269 **Materials and Methods**

### 270 *Specimen collection*

271 Seven fossil mollusc specimens were collected by one of the authors (Stijn Goolaerts) for analysis from  
272 temporary exposures of the Oorderen Member of the Lillo Formation in the Antwerp area, (Belgium, see  
273 **Fig. 1**). These were specimens of *Angulus benedeni benedeni* (specimen ID: SG126 and SG127) from  
274 Deurganckdoksluis (51°16'49"N, 4°14'56"E; collected in 2013), *Pecten complanatus* (SG115) and  
275 *Glycymeris radiolyrata* (SG116) from Deurganckdok (51°17'24"N, 4°15'37"E; collected on Feb 2<sup>nd</sup>, 2001)  
276 *Pygocardia rustica* (SG105), *Ostrea edulis* (SG113), and *Arctica islandica* (SG107) from Verrebroekdok  
277 (51°16'16"N, 4°12'53"E; collected in 1999-2000). At these localities, the Oorderen Member, from  
278 bottom to top, is divided into: basal shell bed, *Atrina* level, *Cultellus* level (SG115 and SG116) and  
279 *benedeni* level (SG126 and SG127)<sup>37</sup>. Specimens SG105, SG113 and SG107 were collected *ex situ* within  
280 the Oorderen Member. The estimated age range for the Oorderen Member is 2.72 Ma – 3.3 Ma<sup>35,40</sup> (see  
281 **Supplementary Information Figure S2**).

### 282 *Palaeoenvironmental context*

283 Field observations and a detailed assessment of the composition of the invertebrate fauna reveal that  
284 the fossil-bearing sediments of the Oorderen Member were deposited between 30 m and 50 m water  
285 depth during warm, highstand intervals within this time window<sup>35,36</sup>. Previous studies have argued that  
286 the SNS undergoes summer stratification during the mPWP that would cause molluscan shell  
287 reconstructions to underestimate summer temperatures<sup>49</sup>. However, the lack of dysoxic faunas in the  
288 Oorderen Member suggests the absence of persistent stratification<sup>35</sup>. Furthermore, the presence of  
289 sedimentary structures indicative of tidal currents and strong vertical mixing during deposition of the  
290 Oorderen Member argues against a large surface to seafloor temperature gradient<sup>39</sup>. Therefore, it is  
291 likely that the molluscs recorded temperatures close to the sea surface temperatures year-round. This  
292 assessment is supported by the observation of warm spring and cool autumn temperatures, suggesting  
293 a direct response of the water temperature experienced by the molluscs to the seasonal cycle in surface  
294 air temperatures (see **Results**; **Fig. 3**). However, given this evidence, we cannot fully exclude that  
295 spatially and temporary restricted temperature stratification did occur during the lifetime of the studied  
296 specimens<sup>49</sup>. Note that, even if summer stratification occurred, the summer temperatures recorded by  
297 the molluscs would underestimate the true mPWP summer SST and the occurrence of enhanced  
298 summer warming during the mPWP would still be supported by the data.

### 299 *Specimen preparation*

300 Shells were partially embedded in epoxy resin before polished thick sections were prepared to expose a  
301 cross section through the axis of maximum shell growth (following<sup>69</sup>; see **Supplementary Information**  
302 **Figure S3**). Preservation of the original shell calcite and aragonite was verified using a combination of  
303 Scanning Electron Microscopy (SEM), cathodoluminescence microscopy (CL), Electron Backscatter  
304 Diffraction microscopy (EBSD), micro-X-ray fluorescence ( $\mu$ XRF) and X-ray Diffraction (XRD; see<sup>40</sup> and  
305 **Supplementary Information Figures S4-S12**). Only shells with excellent preservation as demonstrated by  
306 these methods were considered for clumped isotope analysis.

307

308 *Geochemical analysis*

309 Carbonate was sampled along transects in the direction of growth in transects on cross sections through  
310 the outer shell layers of all shells except *Pecten complanatus* (SG115) and *Angulus benedeni* (SG126 and  
311 SG127), whose thin outer shell layers necessitated sampling on the outside of the ventral margin. A  
312 combination of hand-held drilling (outside) and micromilling (in transects) was used to sample along the  
313 growth increments to minimize time averaging (**Supplementary Information**). The number of samples  
314 per specimen ranges from 61 to 157 (**Fig. 2**): SG105, n = 98; SG107, n = 63; SG113, n = 90; SG115, n =  
315 100; SG116, n = 157; SG126, n = 79; SG127, n = 61). Small (70-160  $\mu\text{g}$ ) aliquots of each sample were  
316 digested in phosphoric acid for 600 seconds at 70°C in a Kiel IV carbonate preparation device, after  
317 which the resultant CO<sub>2</sub> gas was purified using two cold fingers and a Porapak trap<sup>70</sup> before the clumped  
318 isotope composition ( $\Delta_{47}$ ) was analysed using two Thermo MAT253 mass spectrometers. A Long-  
319 Integration Dual Inlet (LIDI) workflow<sup>70,71</sup> was used for all except 53 aliquots from *Pygocardia rustica*  
320 (SG105), the latter of which were measured using sample-standard measurement cycles (“click-clack”  
321 mode; e.g. <sup>72</sup>). Isotopic ratios were standardized using the ETH standards<sup>73</sup>, which were run in  
322 approximately one-to-one ratio with the samples<sup>74</sup> and corrected for <sup>17</sup>O concentration following<sup>75</sup>.  
323 Long-term analytical precision was monitored using IAEA-C2 and Merck reference materials (typical  
324 standard deviation of 0.04‰; see **Supplementary Information Table S2**) after outlier removal based on  
325 metadata on instrument performance (see criteria in **Supplementary Information Section 3.2**).

326 *Seasonality reconstructions*

327 For each mollusk specimen, samples were internally dated relative to the seasonal cycle using  
328 ShellChron<sup>76</sup>, after which measurements within a specimen were grouped in four three-monthly bins  
329 (“seasons”). Summer and winter seasons were defined as consecutive three-month periods with lowest  
330 and highest  $\Delta_{47}$  values, respectively, calculated separately for each specimen (see **Supplementary**  
331 **Information Section 3.2** and **Figures S20-S32**). Mean seasonal  $\Delta_{47}$  values were obtained through  
332 weighted averages of seasonal means and uncertainties considering uncertainty within and variability  
333 between specimens. Seasonal temperatures during the mPWP were reconstructed from  $\Delta_{47}$  for each  
334 seasonal group using the clumped isotope calibration by <sup>77</sup>, propagating uncertainty on  $\Delta_{47}$  values  
335 following the procedure described in the supplement of <sup>78</sup>.

336 *Climate model output*

337 Seasonal SST from the SNS was extracted from the corresponding local ocean grid cells (51-55°N, 2-4°E)  
338 in the PlioMIP2 model ensemble (see **Fig. 2**). SNS SST records were obtained from the same area within  
339 the ERSSTv5 product<sup>43</sup> and supplemented with local SST observations from the NIOZ monitoring  
340 station<sup>44</sup>. Future projections matching the SSP2-4.5 scenario<sup>50</sup> were produced for CMIP6 and the  
341 regional SST outcomes were exported from the IPCC WG1 Interactive Atlas<sup>79</sup>. Seasons were defined as  
342 weighted means of the three months containing the largest number of days in the season according to  
343 the astronomical definition: Winter: January-March, spring: April-June, summer: July-September,  
344 Autumn: October-December. Data processing was carried out using the open-source computational  
345 software R<sup>80</sup> and scripts are provided in <sup>81</sup>.

346

347 **References**

- 348 1. Haywood, A. M., Dowsett, H. J. & Dolan, A. M. Integrating geological archives and climate models  
349 for the mid-Pliocene warm period. *Nat Commun* **7**, 10646 (2016).
- 350 2. Dowsett, H. J. *et al.* Sea Surface Temperature of the mid-Piacenzian Ocean: A Data-Model  
351 Comparison. *Sci Rep* **3**, 2013 (2013).
- 352 3. de la Vega, E., Chalk, T. B., Wilson, P. A., Bysani, R. P. & Foster, G. L. Atmospheric CO<sub>2</sub> during the  
353 Mid-Piacenzian Warm Period and the M2 glaciation. *Sci Rep* **10**, 1–8 (2020).
- 354 4. IPCC. *Climate Change 2021: The Physical Science Basis. Contribution of Working Group I to the Sixth*  
355 *Assessment Report of the Intergovernmental Panel on Climate Change.* (Cambridge University Press,  
356 2021).
- 357 5. Meinshausen, M. *et al.* The shared socio-economic pathway (SSP) greenhouse gas concentrations  
358 and their extensions to 2500. *Geoscientific Model Development* **13**, 3571–3605 (2020).
- 359 6. Liang, Y., Gillett, N. P. & Monahan, A. H. Climate Model Projections of 21st Century Global Warming  
360 Constrained Using the Observed Warming Trend. *Geophysical Research Letters* **47**, e2019GL086757  
361 (2020).
- 362 7. Burke, K. D. *et al.* Pliocene and Eocene provide best analogs for near-future climates. *PNAS* **115**,  
363 13288–13293 (2018).
- 364 8. Climate Action Tracker. 2100 Warming Projections: Emissions and expected warming based on  
365 pledges and current policies. <https://climateactiontracker.org/global/temperatures/> (2022).
- 366 9. Haywood, A. M. *et al.* A return to large-scale features of Pliocene climate: the Pliocene Model  
367 Intercomparison Project Phase 2. *Climate of the Past* (2020).
- 368 10. Cohen, J. *et al.* Recent Arctic amplification and extreme mid-latitude weather. *Nature Geosci* **7**, 627–  
369 637 (2014).

- 370 11. Coumou, D., Lehmann, J. & Beckmann, J. The weakening summer circulation in the Northern  
371 Hemisphere mid-latitudes. *Science* **348**, 324–327 (2015).
- 372 12. Hofer, S., Tedstone, A. J., Fettweis, X. & Bamber, J. L. Decreasing cloud cover drives the recent mass  
373 loss on the Greenland Ice Sheet. *Science Advances* **3**, e1700584 (2017).
- 374 13. Rousi, E., Selten, F., Rahmstorf, S. & Coumou, D. Changes in North Atlantic Atmospheric Circulation  
375 in a Warmer Climate Favor Winter Flooding and Summer Drought over Europe. *Journal of Climate*  
376 **34**, 2277–2295 (2021).
- 377 14. Coumou, D., Di Capua, G., Vavrus, S., Wang, L. & Wang, S. The influence of Arctic amplification on  
378 mid-latitude summer circulation. *Nat Commun* **9**, 2959 (2018).
- 379 15. Dowsett, H. J. *et al.* Sea surface temperatures of the mid-Piacenzian Warm Period: A comparison of  
380 PRISM3 and HadCM3. *Palaeogeography, Palaeoclimatology, Palaeoecology* **309**, 83–91 (2011).
- 381 16. Herbert, T. D., Peterson, L. C., Lawrence, K. T. & Liu, Z. Tropical Ocean Temperatures Over the Past  
382 3.5 Million Years. *Science* **328**, 1530–1534 (2010).
- 383 17. Lawrence, K. T., Sosdian, S., White, H. E. & Rosenthal, Y. North Atlantic climate evolution through  
384 the Plio-Pleistocene climate transitions. *Earth and Planetary Science Letters* **300**, 329–342 (2010).
- 385 18. Wit, J. C., Reichert, G.-J., A Jung, S. J. & Kroon, D. Approaches to unravel seasonality in sea surface  
386 temperatures using paired single-specimen foraminiferal  $\delta^{18}\text{O}$  and Mg/Ca analyses.  
387 *Paleoceanography* **25**, (2010).
- 388 19. Jia, G., Wang, X., Guo, W. & Dong, L. Seasonal distribution of archaeal lipids in surface water and its  
389 constraint on their sources and the TEX86 temperature proxy in sediments of the South China Sea.  
390 *Journal of Geophysical Research: Biogeosciences* **122**, 592–606 (2017).
- 391 20. Conte, M. H. *et al.* Global temperature calibration of the alkenone unsaturation index (UK'37) in  
392 surface waters and comparison with surface sediments. *Geochemistry, Geophysics, Geosystems* **7**,  
393 (2006).

- 394 21. Tindall, J. C., Haywood, A. M., Salzmann, U., Dolan, A. M. & Fletcher, T. The warm winter paradox in  
395 the Pliocene northern high latitudes. *Climate of the Past* **18**, 1385–1405 (2022).
- 396 22. Moss, D. K., Ivany, L. C. & Jones, D. S. Fossil bivalves and the sclerochronological reawakening.  
397 *Paleobiology* **47**, 551–573 (2021).
- 398 23. Schöne, B. R. & Fiebig, J. Seasonality in the North Sea during the Allerød and Late Medieval Climate  
399 Optimum using bivalve sclerochronology. *International Journal of Earth Sciences* **98**, 83–98 (2009).
- 400 24. Johnson, A. L. A., Valentine, A. M., Schöne, B. R., Leng, M. J. & Goolaerts, S. Sclerochronological  
401 evidence of pronounced seasonality from the late Pliocene of the southern North Sea basin and its  
402 implications. *Climate of the Past* **18**, 1203–1229 (2022).
- 403 25. Reynolds, D. J. *et al.* Annually resolved North Atlantic marine climate over the last millennium.  
404 *Nature communications* **7**, 13502 (2016).
- 405 26. de Winter, N. J. *et al.* Absolute seasonal temperature estimates from clumped isotopes in bivalve  
406 shells suggest warm and variable greenhouse climate. *Commun Earth Environ* **2**, 1–8 (2021).
- 407 27. de Winter, N. J. *et al.* An assessment of latest Cretaceous *Pycnodonte vesicularis* (Lamarck, 1806)  
408 shells as records for palaeoseasonality: a multi-proxy investigation. *Climate of the Past* **14**, 725–749  
409 (2018).
- 410 28. Ivany, L. C. Reconstructing paleoseasonality from accretionary skeletal carbonates—challenges and  
411 opportunities. *The Paleontological Society Papers* **18**, 133–166 (2012).
- 412 29. Smale, D. A. *et al.* Marine heatwaves threaten global biodiversity and the provision of ecosystem  
413 services. *Nat. Clim. Chang.* **9**, 306–312 (2019).
- 414 30. Garrabou, J. *et al.* Marine heatwaves drive recurrent mass mortalities in the Mediterranean Sea.  
415 *Global Change Biology* **28**, 5708–5725 (2022).
- 416 31. Manes, S. *et al.* Endemism increases species' climate change risk in areas of global biodiversity  
417 importance. *Biological Conservation* **257**, 109070 (2021).

- 418 32. Toimil, A., Losada, I. J., Nicholls, R. J., Dalrymple, R. A. & Stive, M. J. F. Addressing the challenges of  
419 climate change risks and adaptation in coastal areas: A review. *Coastal Engineering* **156**, 103611  
420 (2020).
- 421 33. Huyghe, D. *et al.* Clumped isotopes in modern marine bivalves. *Geochimica et Cosmochimica Acta*  
422 **316**, 41–58 (2021).
- 423 34. de Winter, N. J. *et al.* Temperature Dependence of Clumped Isotopes ( $\Delta 47$ ) in Aragonite.  
424 *Geophysical Research Letters* **49**, e2022GL099479 (2022).
- 425 35. Wesselingh, F. P., Busschers, F. S. & Goolaerts, S. Observations on the Pliocene sediments exposed  
426 at Antwerp International Airport (northern Belgium) constrain the stratigraphic position of the  
427 Broechem fauna. *Geologica Belgica* (2020).
- 428 36. Marquet, R. Ecology and evolution of Pliocene bivalves from the Antwerp Basin. *Bulletin de l'Institut*  
429 *royal des Sciences naturelles de Belgique, Sciences de la Terre* **74**, 205–212 (2004).
- 430 37. Vandenberghe, N. & Louwye, S. An introduction to the Neogene stratigraphy of northern Belgium:  
431 present status. *Geologica Belgica* **23**, 97–112 (2020).
- 432 38. Quante, M. & Colijn, F. *North Sea region climate change assessment*. (Springer Nature, 2016).
- 433 39. Deckers, J., Louwye, S. & Goolaerts, S. The internal division of the Pliocene Lillo Formation :  
434 correlation between Cone Penetration Tests and lithostratigraphic type sections. *GEOLOGICA*  
435 *BELGICA* **23**, 333–343 (2020).
- 436 40. Wichern, N. M. A. *et al.* The fossil bivalve *Angulus benedeni benedeni*: a potential  
437 seasonally resolved stable isotope-based climate archive to investigate Pliocene temperatures in the  
438 southern North Sea basin. *EGU sphere* 1–53 (2022) doi:10.5194/egusphere-2022-951.
- 439 41. Dowsett, H. *et al.* The PRISM4 (mid-Piacenzian) paleoenvironmental reconstruction. *Climate of the*  
440 *Past* **12**, 1519–1538 (2016).

- 441 42. Lisiecki, L. E. & Raymo, M. E. A Pliocene-Pleistocene stack of 57 globally distributed benthic  $\delta^{18}\text{O}$   
442 records. *Paleoceanography* **20**, (2005).
- 443 43. Huang, B. *et al.* NOAA extended reconstructed sea surface temperature (ERSST), version 5. *NOAA*  
444 *National Centers for Environmental Information* **30**, 25 (2017).
- 445 44. van Aken, H. M. Variability of the water temperature in the western Wadden Sea on tidal to  
446 centennial time scales. *Journal of Sea Research* **60**, 227–234 (2008).
- 447 45. de Nooijer, W. *et al.* Evaluation of Arctic warming in mid-Pliocene climate simulations. *Climate of*  
448 *the Past* **16**, 2325–2341 (2020).
- 449 46. Song, Z., Latif, M., Park, W. & Zhang, Y. Influence of Model Bias on Simulating North Atlantic Sea  
450 Surface Temperature During the Mid-Pliocene. *Paleoceanography and Paleoclimatology* **33**, 884–  
451 893 (2018).
- 452 47. Cook, F. *et al.* Marine heatwaves in shallow coastal ecosystems are coupled with the atmosphere:  
453 Insights from half a century of daily in situ temperature records. *Frontiers in Climate* **4**, (2022).
- 454 48. Sharples, J., Ross, O. N., Scott, B. E., Greenstreet, S. P. R. & Fraser, H. Inter-annual variability in the  
455 timing of stratification and the spring bloom in the North-western North Sea. *Continental Shelf*  
456 *Research* **26**, 733–751 (2006).
- 457 49. Valentine, A., Johnson, A. L. A., Leng, M. J., Sloane, H. J. & Balson, P. S. Isotopic evidence of cool  
458 winter conditions in the mid-Piacenzian (Pliocene) of the southern North Sea Basin.  
459 *Palaeogeography, Palaeoclimatology, Palaeoecology* **309**, 9–16 (2011).
- 460 50. O’Neill, B. C. *et al.* The Scenario Model Intercomparison Project (ScenarioMIP) for CMIP6.  
461 *Geoscientific Model Development* **9**, 3461–3482 (2016).
- 462 51. Tierney, J. E. *et al.* Past climates inform our future. *Science* **370**, (2020).
- 463 52. Byrne, M. P. & O’Gorman, P. A. Trends in continental temperature and humidity directly linked to  
464 ocean warming. *Proceedings of the National Academy of Sciences* **115**, 4863–4868 (2018).

- 465 53. Clotten, C., Stein, R., Fahl, K. & De Schepper, S. Seasonal sea ice cover during the warm Pliocene:  
466 Evidence from the Iceland Sea (ODP Site 907). *Earth and Planetary Science Letters* **481**, 61–72  
467 (2018).
- 468 54. Knies, J. *et al.* The emergence of modern sea ice cover in the Arctic Ocean. *Nat Commun* **5**, 5608  
469 (2014).
- 470 55. Haine, T. W. N. & Martin, T. The Arctic-Subarctic sea ice system is entering a seasonal regime:  
471 Implications for future Arctic amplification. *Sci Rep* **7**, 4618 (2017).
- 472 56. Dai, A., Luo, D., Song, M. & Liu, J. Arctic amplification is caused by sea-ice loss under increasing CO<sub>2</sub>.  
473 *Nat Commun* **10**, 121 (2019).
- 474 57. Kyselý, J. & Huth, R. Changes in atmospheric circulation over Europe detected by objective and  
475 subjective methods. *Theor. Appl. Climatol.* **85**, 19–36 (2006).
- 476 58. Kyselý, J. Influence of the persistence of circulation patterns on warm and cold temperature  
477 anomalies in Europe: Analysis over the 20th century. *Global and Planetary Change* **62**, 147–163  
478 (2008).
- 479 59. Stott, P. A. *et al.* Attribution of extreme weather and climate-related events. *WIREs Climate Change*  
480 **7**, 23–41 (2016).
- 481 60. Schuldt, B. *et al.* A first assessment of the impact of the extreme 2018 summer drought on Central  
482 European forests. *Basic and Applied Ecology* **45**, 86–103 (2020).
- 483 61. Steirou, E., Gerlitz, L., Apel, H., Sun, X. & Merz, B. Climate influences on flood probabilities across  
484 Europe. *Hydrology and Earth System Sciences* **23**, 1305–1322 (2019).
- 485 62. Kamenos, N. A. North Atlantic summers have warmed more than winters since 1353, and the  
486 response of marine zooplankton. *Proceedings of the National Academy of Sciences* **107**, 22442–  
487 22447 (2010).

- 488 63. Schär, C. *et al.* The role of increasing temperature variability in European summer heatwaves.  
489 *Nature* **427**, 332–336 (2004).
- 490 64. Frölicher, T. L., Fischer, E. M. & Gruber, N. Marine heatwaves under global warming. *Nature* **560**,  
491 360–364 (2018).
- 492 65. Piatt, J. F. *et al.* Extreme mortality and reproductive failure of common murrelets resulting from the  
493 northeast Pacific marine heatwave of 2014-2016. *PLOS ONE* **15**, e0226087 (2020).
- 494 66. Hughes, T. P. *et al.* Global warming and recurrent mass bleaching of corals. *Nature* **543**, 373–377  
495 (2017).
- 496 67. Scripps Institution of Oceanography *et al.* Biological Impacts of the 2013–2015 Warm-Water  
497 Anomaly in the Northeast Pacific: Winners, Losers, and the Future. *Oceanog* **29**, (2016).
- 498 68. *Climate Change 2022: Impacts, Adaptation and Vulnerability. Contribution of Working Group II to*  
499 *the Sixth Assessment Report of the Intergovernmental Panel on Climate Change.* (2022).
- 500 69. Schöne, B. R. *et al.* Climate records from a bivalved Methuselah (*Arctica islandica*, Mollusca;  
501 Iceland). *Palaeogeography, Palaeoclimatology, Palaeoecology* **228**, 130–148 (2005).
- 502 70. Meckler, A. N., Ziegler, M., Millán, M. I., Breitenbach, S. F. & Bernasconi, S. M. Long-term  
503 performance of the Kiel carbonate device with a new correction scheme for clumped isotope  
504 measurements. *Rapid Communications in Mass Spectrometry* **28**, 1705–1715 (2014).
- 505 71. Müller, I. A. *et al.* Carbonate clumped isotope analyses with the long-integration dual-inlet (LIDI)  
506 workflow: scratching at the lower sample weight boundaries: LIDI as key for more precise analyses  
507 on much less carbonate material. *Rapid Communications in Mass Spectrometry* **31**, 1057–1066  
508 (2017).
- 509 72. Murray, S. T., Arienzo, M. M. & Swart, P. K. Determining the  $\Delta 47$  acid fractionation in dolomites.  
510 *Geochimica et Cosmochimica Acta* **174**, 42–53 (2016).

- 511 73. Bernasconi, S. M. *et al.* Reducing uncertainties in carbonate clumped isotope analysis through  
512 consistent carbonate-based standardization. *Geochemistry, Geophysics, Geosystems* **19**, 2895–2914  
513 (2018).
- 514 74. Kocken, I. J., Müller, I. A. & Ziegler, M. Optimizing the Use of Carbonate Standards to Minimize  
515 Uncertainties in Clumped Isotope Data. *Geochemistry, Geophysics, Geosystems* **20**, 5565–5577  
516 (2019).
- 517 75. Brand, W. A., Assonov, S. S. & Coplen, T. B. Correction for the  $^{17}\text{O}$  interference in  $\delta(^{13}\text{C})$   
518 measurements when analyzing  $\text{CO}_2$  with stable isotope mass spectrometry (IUPAC Technical  
519 Report). *Pure and Applied Chemistry* **82**, 1719–1733 (2010).
- 520 76. de Winter, N. J. ShellChron 0.2.8: A new tool for constructing chronologies in accretionary carbonate  
521 archives from stable oxygen isotope profiles. *Geoscientific Model Development Discussions* 1–37  
522 (2021) doi:<https://doi.org/10.5194/gmd-2020-401>.
- 523 77. Meinicke, N., Reimi, M. A., Ravelo, A. C. & Meckler, A. N. Coupled Mg/Ca and Clumped Isotope  
524 Measurements Indicate Lack of Substantial Mixed Layer Cooling in the Western Pacific Warm Pool  
525 During the Last ~5 Million Years. *Paleoceanography and Paleoclimatology* **36**, e2020PA004115  
526 (2021).
- 527 78. Huntington, K. W. *et al.* Methods and limitations of ‘clumped’  $\text{CO}_2$  isotope ( $\Delta 47$ ) analysis by gas-  
528 source isotope ratio mass spectrometry. *Journal of Mass Spectrometry* **44**, 1318–1329 (2009).
- 529 79. Iturbide, M. *et al.* Implementation of FAIR principles in the IPCC: the WGI AR6 Atlas repository. *Sci*  
530 *Data* **9**, 629 (2022).
- 531 80. R Core Team. *R: A Language and Environment for Statistical Computing*. (R Foundation for Statistical  
532 Computing, 2023).
- 533 81. de Winter, N. J. Supplementary Information to: ‘Amplified seasonality in western Europe in a  
534 warmer world’ submitted to publication. (2023) doi:10.5281/zenodo.8227319.

- 535 82. Schöne, B. R. *et al.* Climate records from a bivalved Methuselah (*Arctica islandica*, Mollusca;  
536 Iceland). *Palaeogeography, Palaeoclimatology, Palaeoecology* **228**, 130–148 (2005).
- 537 83. Schindelin, J. *et al.* Fiji: an open-source platform for biological-image analysis. *Nature methods* **9**,  
538 676–682 (2012).
- 539 84. Cochran, J. K. *et al.* Effect of diagenesis on the Sr, O, and C isotope composition of late Cretaceous  
540 mollusks from the Western Interior Seaway of North America. *American Journal of Science* **310**, 69–  
541 88 (2010).
- 542 85. de Winter, N. J. *et al.* The giant marine gastropod *Campanile giganteum* (Lamarck, 1804) as a high-  
543 resolution archive of seasonality in the Eocene greenhouse world. *Geochemistry, Geophysics,*  
544 *Geosystems* **21**, e2019GC008794 (2020).
- 545 86. Höche, N., Peharda, M., Walliser, E. O. & Schöne, B. R. Morphological variations of crossed-lamellar  
546 ultrastructures of *Glycymeris bimaculata* (Bivalvia) serve as a marine temperature proxy. *Estuarine,*  
547 *Coastal and Shelf Science* **237**, 106658 (2020).
- 548 87. Crippa, G. *et al.* Orientation patterns of aragonitic crossed-lamellar, fibrous prismatic and  
549 myostracal microstructures of modern *Glycymeris* shells. *Journal of Structural Biology* **212**, 107653  
550 (2020).
- 551 88. Janiszewska, K., Mazur, M., Machalski, M. & Stolarski, J. From pristine aragonite to blocky calcite:  
552 Exceptional preservation and diagenesis of cephalopod nacre in porous Cretaceous limestones.  
553 *PLOS ONE* **13**, e0208598 (2018).
- 554 89. Barbin, V. *et al.* Cathodoluminescence of recent biogenic carbonates: environmental and  
555 ontogenetic fingerprint. *Geological Magazine* **128**, 19–26 (1991).
- 556 90. Barbin, V. Cathodoluminescence of carbonate shells: biochemical vs diagenetic process. in  
557 *Cathodoluminescence in Geosciences* 303–329 (Springer, 2000).

- 558 91. Brand, U. & Veizer, J. Chemical diagenesis of a multicomponent carbonate system—1: Trace  
559 elements. *Journal of Sedimentary Research* **50**, (1980).
- 560 92. de Winter, N. J. & Claeys, P. Micro X-ray fluorescence ( $\mu$ XRF) line scanning on Cretaceous rudist  
561 bivalves: A new method for reproducible trace element profiles in bivalve calcite. *Sedimentology* **64**,  
562 231–251 (2016).
- 563 93. Pagel, M., Barbin, V., Blanc, P. & Ohnenstetter, D. *Cathodoluminescence in geosciences*. (Springer  
564 Science & Business Media, 2013).
- 565 94. Götte, T. & Richter, D. K. Quantitative aspects of Mn-activated cathodoluminescence of natural and  
566 synthetic aragonite. *Sedimentology* **56**, 483–492 (2009).
- 567 95. Cusack, M. Biomineral electron backscatter diffraction for palaeontology. *Palaeontology* **59**, 171–  
568 179 (2016).
- 569 96. Casella, L. A. *et al.* Experimental diagenesis: insights into aragonite to calcite transformation of  
570 *Arctica islandica* shells by hydrothermal treatment. *Biogeosciences* **14**, 1461–1492 (2017).
- 571 97. Ritter, A.-C. *et al.* Exploring the impact of diagenesis on (isotope) geochemical and microstructural  
572 alteration features in biogenic aragonite. *Sedimentology* **64**, 1354–1380 (2017).
- 573 98. Marcano, M. C., Frank, T. D., Mukasa, S. B., Lohmann, K. C. & Taviani, M. Diagenetic incorporation of  
574 Sr into aragonitic bivalve shells: implications for chronostratigraphic and palaeoenvironmental  
575 interpretations. *The Depositional Record* **1**, 38–52 (2015).
- 576 99. Popov, S. V. Formation of bivalve shells and their microstructure. *Paleontological Journal* **48**, 1519–  
577 1531 (2014).
- 578 100. Checa, A. G., Esteban-Delgado, F. J. & Rodríguez-Navarro, A. B. Crystallographic structure of the  
579 foliated calcite of bivalves. *Journal of structural biology* **157**, 393–402 (2007).
- 580 101. Freitas, P. S., Clarke, L. J., Kennedy, H., Richardson, C. A., & others. Ion microprobe assessment  
581 of the heterogeneity of Mg/Ca, Sr/Ca and Mn/Ca ratios in *Pecten maximus* and *Mytilus edulis*

582 (bivalvia) shell calcite precipitated at constant temperature. *Biogeosciences Discussions* **6**, 1267  
583 (2009).

584 102. de Winter, N., Sinnesael, M., Makarona, C., Vansteenberge, S. & Claeys, P. Trace element  
585 analyses of carbonates using portable and micro-X-ray fluorescence: Performance and optimization  
586 of measurement parameters and strategies. *Journal of Analytical Atomic Spectrometry* (2017).

587 103. Vellekoop, J. *et al.* A new age model and chemostratigraphic framework for the Maastrichtian  
588 type area (southeastern Netherlands, northeastern Belgium). *Newsletters on Stratigraphy* **55**, 479–  
589 501 (2022).

590 104. Al-Aasm, I. S. & Veizer, J. Diagenetic Stabilization of Aragonite and Low-mg Calcite, I. Trace  
591 Elements in Rudists. *Journal of Sedimentary Research* **56**, (1986).

592 105. Hendry, J. P., Ditchfield, P. W. & D. Marshall, J. Two-Stage Neomorphism of Jurassic Aragonitic  
593 Bivalves: Implications for Early Diagenesis. *Journal of Sedimentary Research* **65**, (1995).

594 106. Carré, M. *et al.* Calcification rate influence on trace element concentrations in aragonitic bivalve  
595 shells: Evidences and mechanisms. *Geochimica et Cosmochimica Acta* **70**, 4906–4920 (2006).

596 107. Lafuente, B., Downs, R. T., Yang, H. & Stone, N. 1. The power of databases: The RRUFF project. in  
597 *Highlights in mineralogical crystallography* 1–30 (De Gruyter (O), 2015).

598 108. Ghosh, P. *et al.* 13C–18O bonds in carbonate minerals: a new kind of paleothermometer.  
599 *Geochimica et Cosmochimica Acta* **70**, 1439–1456 (2006).

600 109. Daëron, M., Blamart, D., Peral, M. & Affek, H. P. Absolute isotopic abundance ratios and the  
601 accuracy of  $\Delta 47$  measurements. *Chemical Geology* **442**, 83–96 (2016).

602 110. IAEA-C-2. *Nucleus* <https://nucleus.iaea.org/sites/ReferenceMaterials>.

603 111. Müller, I. A. *et al.* Calibration of the oxygen and clumped isotope thermometers for (proto-  
604 )dolomite based on synthetic and natural carbonates. *Chemical Geology* **525**, 1–17 (2019).

- 605 112. Bernasconi, S. M. *et al.* InterCarb: A Community Effort to Improve Interlaboratory  
606 Standardization of the Carbonate Clumped Isotope Thermometer Using Carbonate Standards.  
607 *Geochemistry, Geophysics, Geosystems* **22**, e2020GC009588 (2021).
- 608 113. de Winter, N., Agterhuis, T. & Ziegler, M. Optimizing sampling strategies in high-resolution  
609 paleoclimate records. *Climate of the Past Discussions* 1–52 (2020) doi:[https://doi.org/10.5194/cp-](https://doi.org/10.5194/cp-2020-118)  
610 2020-118.
- 611 114. Haywood, A. M. *et al.* The Pliocene Model Intercomparison Project Phase 2: large-scale climate  
612 features and climate sensitivity. *Climate of the Past* **16**, 2095–2123 (2020).
- 613 115. Chandan, D. & Peltier, W. R. Regional and global climate for the mid-Pliocene using the  
614 University of Toronto version of CCSM4 and PlioMIP2 boundary conditions. *Climate of the Past* **13**,  
615 919–942 (2017).
- 616 116. Baatsen, M. L. J., von der Heydt, A. S., Kliphuis, M. A., Oldeman, A. M. & Weiffenbach, J. E. Warm  
617 mid-Pliocene conditions without high climate sensitivity: the CCSM4-Utrecht (CESM 1.0.5)  
618 contribution to the PlioMIP2. *Climate of the Past* **18**, 657–679 (2022).
- 619 117. Stepanek, C., Samakinwa, E., Knorr, G. & Lohmann, G. Contribution of the coupled atmosphere–  
620 ocean–sea ice–vegetation model COSMOS to the PlioMIP2. *Climate of the Past* **16**, 2275–2323  
621 (2020).
- 622 118. Zheng, J., Zhang, Q., Li, Q., Zhang, Q. & Cai, M. Contribution of sea ice albedo and insulation  
623 effects to Arctic amplification in the EC-Earth Pliocene simulation. *Climate of the Past* **15**, 291–305  
624 (2019).
- 625 119. Kelley, M. *et al.* GISS-E2.1: Configurations and Climatology. *Journal of Advances in Modeling*  
626 *Earth Systems* **12**, e2019MS002025 (2020).
- 627 120. Hunter, S. J., Haywood, A. M., Dolan, A. M. & Tindall, J. C. The HadCM3 contribution to PlioMIP  
628 phase 2. *Climate of the Past* **15**, 1691–1713 (2019).

- 629 121. Dufresne, J.-L. *et al.* Climate change projections using the IPSL-CM5 Earth System Model: from  
630 CMIP3 to CMIP5. *Clim Dyn* **40**, 2123–2165 (2013).
- 631 122. Chan, W.-L. & Abe-Ouchi, A. Pliocene Model Intercomparison Project (PlioMIP2) simulations  
632 using the Model for Interdisciplinary Research on Climate (MIROC4m). *Climate of the Past* **16**, 1523–  
633 1545 (2020).
- 634 123. Li, X., Guo, C., Zhang, Z., Otterå, O. H. & Zhang, R. PlioMIP2 simulations with NorESM-L and  
635 NorESM1-F. *Climate of the Past* **16**, 183–197 (2020).
- 636 124. Haywood, A. M. *et al.* The Pliocene Model Intercomparison Project (PlioMIP) Phase 2: scientific  
637 objectives and experimental design. *Climate of the Past* **12**, 663–675 (2016).
- 638 125. Cleveland, W. S., Grosse, E. & Shyu, W. M. Local regression models. in *Statistical models in S*  
639 (Wadsworth & Brooks/Cole, 1992).
- 640 126. Ridderinkhof, H. Tidal and residual flows in the western Dutch Wadden Sea II: An analytical  
641 model to study the constant flow between connected tidal basins. *Netherlands Journal of Sea*  
642 *Research* **22**, 185–198 (1988).
- 643 127. Van Aken, H. M. 140 years of daily observations in a tidal inlet (Marsdiep). *ICES Mar Sci Symp*  
644 **219**, 359–361 (2003).
- 645 128. Van der Hoeven, P. C. T. Observations of surface water temperature and salinity, State Office of  
646 Fishery Research (RIVO): 1860–1981. *KNMI Scientific Report WR* **82**, 2 (1982).
- 647 129. IPCC AR6-WGI Atlas. <https://interactive-atlas.ipcc.ch/atlas>.
- 648 130. IPCC. *Climate change 2013: the physical science basis: Working Group I contribution to the Fifth*  
649 *assessment report of the Intergovernmental Panel on Climate Change*. (Cambridge University Press,  
650 2013).
- 651
- 652

## 653 Acknowledgements

654 This research would not have been possible without the dedicated lab assistance from Arnold van Dijk,  
655 Desmond Eefting, Ilja Kocken and Inigo Müller in the Utrecht University clumped isotope lab. The authors  
656 would like to thank Leonard Bik (UU), Bart Lippens (VUB) and Bauke Lacet (VU Amsterdam) for their help  
657 with sample preparation and Maarten Zeilmans (UU) for his assistance with high-resolution colour scans  
658 of the shell specimens. We thank Tilly Bouten (UU) for help with the SEM analyses, Maartje Hamer (UU)  
659 for assistance with EBSD, João Trabucho Alexandre (UU) and Anita van Leeuwen (UU) for assistance with  
660 XRD analyses, Andre Niemeyer (UU) for his help with cathodoluminescence microscopy and Roald Tagle  
661 (Bruker Nano GmbH), Steven Goderis and Luc Deriemaker (VUB) for their assistance in the AMGC-VUB  
662 XRF lab. NJW thanks Lenette de Gier (UU), Jennifer Franke (UU), and Bram Verhage (UU) for their  
663 assistance with sampling, diagenetic screening and lab analysis. This manuscript benefitted from  
664 discussions with Paolo Scussolini (VU Amsterdam). Stijn Goolaerts is grateful to Veerle Schelfhout, Freddy  
665 Aerts, Murielle Reyns, Roger Sieckelink, and Nouredine Ouifak of “Mobiliteit en Openbare Werken  
666 (MOW)” for granting access to the Verrebroekdok (1999-2000), Deurganckdok (2001-2002) and  
667 Deurganckdoksluis (2012–2014) construction sites, allowing the collection of the study material.

668 This work was funded through a Marie Curie Individual Fellowship (grant no. H2020-MSCA-IF-2018 -  
669 UNBIAS, 843011) and Flemish research Council (FWO) postdoctoral fellowship (grant no. 12ZB220N), both  
670 awarded to NJW. BG is supported by an UU-NIOZ collaboration grant. AJ is supported by a grant from the  
671 Leverhulme Trust (RPG-2021-090). PK was supported by FWO PhD fellowship 11E6621N. PC thanks the  
672 VUB Strategic Research Program for support, as well as the FWO - Hercules Program for financing the  
673  $\mu$ XRF instrument at AMGC.

674 Below is an overview of author contributions according to the CRediT framework: This study was  
675 conceptualized by NJW, PC and MZ. Data curation was done by NJW, JT, BG, NW, SL, BM and MZ. Formal  
676 analysis was carried out by NJW. Funding for the project was acquired by NJW, PC and MZ. Investigation  
677 and experimental work were done by NJW, BG, NW, PK, FH and MZ. NJW, JT and MZ were responsible for  
678 development of the methodology. The project was managed by NJW under supervision by PC and MZ.  
679 Resources were provided by SG and FW. Development of software for formal analysis was by NJW. NJW,  
680 AJ, PC and MZ supervised the project. Validation of the reproducibility of the results was by NJW, JT, BG,  
681 PK, FH, SL, BM, PB, FW and MZ. Visualization of the results was initiated by NJW, JT, NW and FW and  
682 improved through contributions from AJ, BG, BM, PB and MZ. The original draft was written by NJW. All  
683 authors contributed to reviewing and editing subsequent versions of the manuscript.

684 The authors declare that they have no competing interests. All data on which this study is based are made  
685 available through the open-access database Zenodo: <https://doi.org/10.5281/zenodo.8378900>.

686